Finite response time of shock wave modulation by turbulence

Kento Inokuma, Tomoaki Watanabe, Koji Nagata, Akihiro Sasoh, and Yasuhiko Sakai

Citation: Physics of Fluids **29**, 051701 (2017); doi: 10.1063/1.4982932
View online: http://dx.doi.org/10.1063/1.4982932
View Table of Contents: http://aip.scitation.org/toc/phf/29/5
Published by the American Institute of Physics

Finite response time of shock wave modulation by turbulence

Kento Inokuma,[1] Tomoaki Watanabe,[1,a)] Koji Nagata,[1] Akihiro Sasoh,[1] and Yasuhiko Sakai[2]
[1]*Department of Aerospace Engineering, Nagoya University, Nagoya, Japan*
[2]*Department of Mechanical Science and Engineering, Nagoya University, Nagoya, Japan*

(Received 9 March 2017; accepted 21 April 2017; published online 5 May 2017)

Response time of the post-shock wave (SW) overpressure modulation by turbulence is investigated in wind tunnel experiments. A peak-overpressure fluctuation, observed on a wall, is induced by turbulence around the SW ray, but away from the wall, demonstrating finite response time of the modulation. We propose a model of the modulation based on the SW deformation by a local flow disturbance, which yields the response time being proportional to the product of the large-eddy turnover time and $(M_T/M_{S0})^{0.5}$ (M_T: turbulent Mach number and M_{S0}: shock Mach number), in consistent with the experiments. *Published by AIP Publishing.* [http://dx.doi.org/10.1063/1.4982932]

The interaction between turbulence and a shock wave (SW) is an important problem in a wide range of scientific fields (e.g., star formations in galaxies[1] and inertial confinement fusion[2]). Engineering applications also face this problem such as in supersonic transports generating sonic booms, which have a large influence on our living environment and wildlife.[3] One of interesting problems in shock/turbulence interactions is the modulation of the SW, which has been observed as a post-SW overpressure fluctuation induced by turbulence.[4–7] It has been found that the level of induced post-SW overpressure fluctuation depends on the turbulence intensity. However, since the characteristics of turbulence and SW were not obtained simultaneously in most previous experiments, the relation remains unclear between the turbulence and the SW modulation. Detailed investigations require simultaneous and quantitative measurements of SW and turbulence, which is characterized by spatiotemporal fluctuations with a wide range of scales of motions.

We investigate the effects of turbulence, generated by a grid, on the overpressure behind a spherical SW by means of wind tunnel experiments. We estimate a spatial distribution of turbulence, where the post-SW overpressure is modulated during the propagation. The detail of the wind tunnel can be found in Refs. 6 and 8. Figure 1(a) describes the experimental setup. Grid turbulence is generated with square grids with a mesh size M (solidity: 0.36) installed at the entrance to the test section. U_0 denotes the streamwise mean velocity of the grid turbulence. A spherical SW is ejected vertically downward from an open end of a tube using a quick piston valve.[6] The total length and the inner diameter of the tube are 3.4 m and 23.3 mm, respectively. Between the grid and the open end of the shock tube we install a measurement plate with the thickness of 5 mm, on which a piezoelectric pressure transducer (PCB Piezotronics, Inc., 113B27) and an I-type hot-wire probe (DANTEC DYNAMICS 55P11) are mounted (see Fig. 1(a)) for the measurements of overpressure $P(t)$ on the plate and streamwise velocity $U(t)$. The measurement plate is fixed 75 mm above the wall of the wind tunnel to prevent the boundary layer from affecting the measurements. The pressure transducer is mounted near the edge of the plate so that the pressure measurement is not affected by the growth of the Mach stem. The shock Mach number is set to $M_{S0} = 1.004$ on the measurement plate. The experimental conditions are summarized in Table I, which also includes turbulence characteristics at the velocity measurement location. Further details of grid turbulence studied here can be found in Ref. 8. With the SW generator and the measurement system controlled by a computer, the sampling of the signals of $P(t)$ and $U(t)$ with the oscilloscope (YOKOGAWA DL 750) at a sampling rate 1 MHz is started 50 ms before the SW is ejected from the open end. The velocity measurement height h defined in Fig. 1(a) is ranged from 15 mm to 125 mm. In each measurement condition, 500 runs of the SW were used for the statistical analysis. Note that the statistics with 300 runs yield qualitatively the same results discussed below.

Figure 1(b) shows examples of time histories of P. The increase in P due to the SW is defined as peak-overpressure Δp with the peak value of P, and its fluctuation $\Delta p''$ is defined with $\Delta p'' = \Delta p - \langle \Delta p \rangle$. Here, $\langle\ \rangle$ denotes the ensemble average of all runs of the SW. We analyze Δp and $U(t)$ before the SW reaches the measurement plate.

The rms value of the velocity fluctuation u $(=U(t) - U_0)$ and that of the peak-overpressure fluctuation $\Delta p''$ are shown in Table I as u_{rms} and p_{rms}. We can find that p_{rms} increases with u_{rms}, in agreement with previous studies.[4,6,7]

With the Taylor hypothesis, the spatial distribution of the velocity $U(d)$ at h can be estimated from $U(t)$ at the moment when the SW is ejected, where d is the streamwise distance from the pressure transducer (see Fig. 1(a)). The decay of grid-turbulence is not important in the range of d considered here.[8] Since the fluid motion is much slower than the SW propagation, the turbulence can be assumed to be frozen and hardly changes while the SW is propagating. Thus, the SW propagates upstream through the turbulence, whose velocity profile at h is represented by $U(d)$, and reaches the pressure transducer location. Furthermore, the low pass filtered velocity with a cutoff length Δd is calculated as $\bar{U}(d, \Delta d)$

a)watanabe.tomoaki@c.nagoya-u.jp

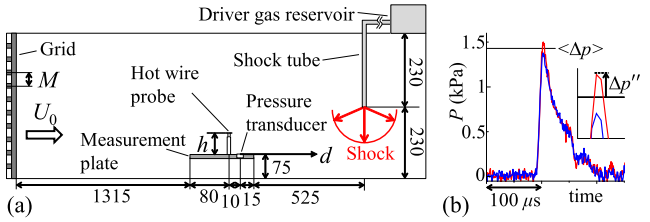

FIG. 1. (a) Experimental setup. Lengths are shown in mm. (b) Examples of time histories of overpressure P for M100-U10. Red/blue line shows strong/weak case. The ensemble average of peak overpressure $\langle\Delta p\rangle$ and peak-overpressure fluctuation $\Delta p'' = \Delta p - \langle\Delta p\rangle$ is also shown.

$= (1/\Delta d)\int_{-\Delta d/2}^{\Delta d/2} U(d+\delta)\mathrm{d}\delta$, which is the velocity of motions in scales larger than Δd at the location d. Thus, we are able to investigate the relation between the overpressure and the turbulent motions at the location d with scales larger than Δd.

To evaluate the relation between the velocity fluctuation and the peak-overpressure fluctuation, the correlation coefficient defined with the ensemble average is calculated for $\Delta p''$ and $\bar{u}(d,\Delta d)$ $(=\bar{U}(d,\Delta d) - U_0)$ at the height h as $R(d,\Delta d) = \langle \bar{u}\Delta p''\rangle / \sqrt{\langle(\bar{u})^2\rangle\langle(\Delta p'')^2\rangle}$. Figure 2 shows R for M100-U10, where the velocity and peak-overpressure fluctuations are found to be positively correlated. Similar profiles of $R(d,\Delta d)$ were also obtained for all cases. A high correlation can be observed for the velocity fluctuation at a specific location d and scale Δd. We define a maximum value of R as $R_{\max} = R(d_{\max}, \Delta d_{\max})$, which is denoted by the crosses in Fig. 2. We can find a strong dependence of $d_{\max}$ on h while an h-dependence of $\Delta d_{\max}$ is not very clear. $\Delta d_{\max}$ in each figure suggests that turbulent motions which affect the peak overpressure are related to the large scales, which is of the order of an integral length scale (see Table I). Figure 3 plots $d_{\max}$ against h compared with the SW ray toward the pressure transducer location. The plots are mostly on the ray, which indicates that the peak overpressure is affected by the turbulence around the ray.

Figure 4 shows the relation between $d_{\max}$ and $R_{\max}$ at different h for all cases. $R_{\max}$ decreases with $d_{\max}$ after it has reached the maximum, confirming that the turbulence very far

TABLE I. Experimental conditions of grid turbulence and the rms peak-overpressure fluctuation p_{rms} induced by grid turbulence. The mesh Reynolds number is defined with $Re_M = U_0 M/\nu$, where ν is the kinematic viscosity. The table also includes the rms streamwise velocity fluctuation u_{rms}, Kolmogorov microscale η, Taylor microscale λ, and longitudinal integral length scale L_u, at the measurement location. The definitions of scales can be seen in Reference 8.

Case	M50-U10	M50-U20	M100-U10	M100-U20
Symbol	△ (blue)	○ (green)	▽ (black)	□ (red)
M (mm)	50	50	100	100
U_0 (m/s)	10	20	10	20
Re_M	3.35×10^4	6.7×10^4	6.7×10^4	13.4×10^4
η (mm)	0.198	0.134	0.163	0.112
λ (mm)	3.92	3.75	3.91	3.78
L_u (mm)	27.5	48.1	54.3	64.3
u_{rms} (m/s)	0.387	0.798	0.568	1.17
$p_{\mathrm{rms}}/\langle\Delta p\rangle$	0.0269	0.0620	0.0338	0.0703

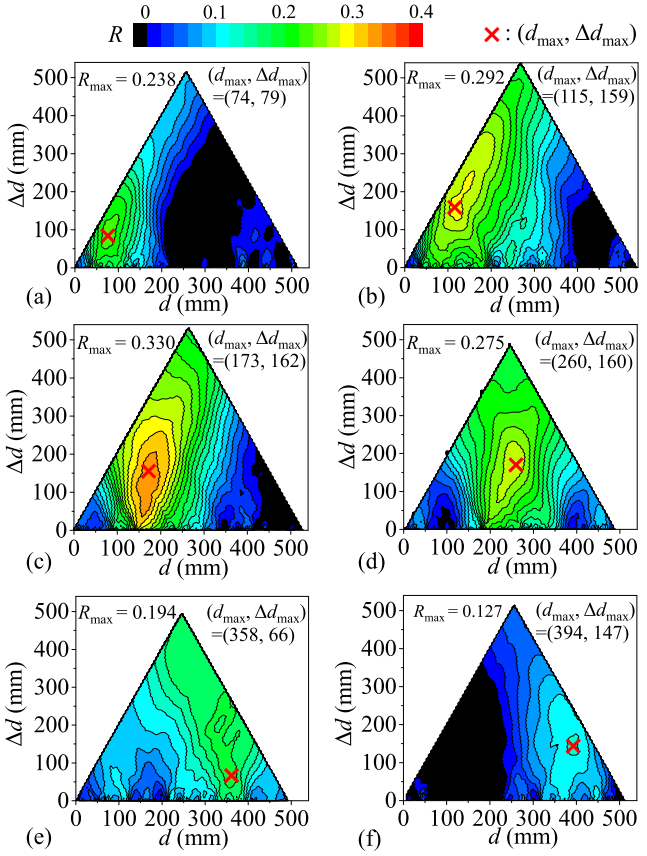

FIG. 2. Correlation coefficients $R(d,\Delta d)$ between the peak-overpressure fluctuation and velocity fluctuation for M100-U10 measured at h of (a) 15 mm, (b) 25 mm, (c) 50 mm, (d) 75 mm, (e) 100 mm, and (f) 125 mm. The crosses show $(d,\Delta d) = (d_{\max}, \Delta d_{\max})$, where R has a maximum value $R_{\max}$ in each figure.

away from the pressure transducer location has a small influence on the peak overpressure. Since the SW is continuously affected by turbulence during the propagation, the influences of turbulence on the SW modulation at an earlier time of the propagation are somehow negated by turbulence near the pressure transducer location.

Interestingly, the strongest correlation is not related to the smallest $d_{\max}$ (the smallest h) but is observed at some distance away from the pressure transducer location. Thus, it takes finite time for the post-SW overpressure to change after the SW is interfered with turbulence. The concept of the response time is consistent with numerical simulations of shock/vortex interactions,[9] where the SW deformation by the vortex is more significant slightly after the SW has passed the vortex than while the SW is propagating within the vortex (the deformation

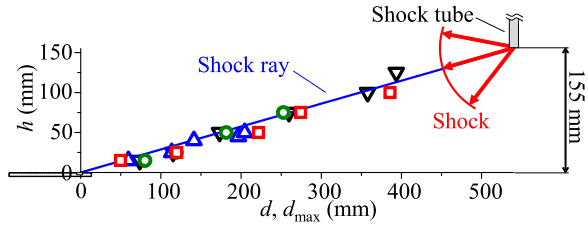

FIG. 3. Relation between $d_{\max}$ and h. Blue line shows the SW ray along which the SW propagates toward the pressure transducer location ($d = 0$, $h = 0$). See Table I for symbols.

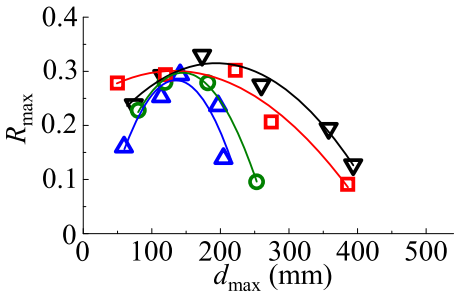

FIG. 4. Relation between d_{max} and R_{max}. Solid lines are quadratic approximations. See Table I for symbols.

can cause the post-SW overpressure modulation[10]). We introduce d_P, which is the value of d_{max} corresponding to a maximum value of R_{max} in Fig. 4, where d_P is estimated with the quadratic fitting. d_P can be related to the time required for the turbulent effects on the overpressure to be the most significant. Apparently, the response distance d_P in all cases is much larger than η and λ (Table I), and the integral length/time scale might be an appropriate quantity of turbulence characterizing the response distance/time.

We estimate the response distance/time of the post-SW overpressure modulation by turbulence with a simple model of axisymmetric deformation of a SW by a local flow disturbance. We consider a plane SW with the shock Mach number M_{S0} and the propagation velocity $U_{S0} = M_{S0}a$ (a: the sound speed in front of the SW) at the initial state ($t = 0$), which encounters the velocity fluctuation centered at $r = 0$ as in Fig. 5. A circular control area A embedded on the SW at $t = 0$ changes with the SW deformation. The perimeter of A is tracked along the SW ray with the shock propagation, whose direction is locally normal to the SW. We now estimate a temporal variation of A by the velocity fluctuation $u(r)$ characterized by u_{rms} and lateral integral length scale L, which is related to the large-scale turbulent motions. Positive u denotes the velocity against the SW propagation direction. We can write $u(r)$ as $u_{rms}f(\tilde{r})$ ($\tilde{r} = r/L$) with a dimensionless function f, where for positive u, $f(0) = 1$ and $f(r)$ monotonically decreases to 0 with r. Similarly, negative u is represented with $f(r)$ which monotonically increases from $f(0) = -1$ to 0 with r. We consider $\partial f/\partial x = 0$ in the model since the velocity gradient in the r direction causes a larger SW deformation than in the x direction in this model. The non-uniform SW motion by $u(r)$ causes the SW surface to be inclined, where an angle between the x axis and the SW ray is $\theta(r, t)$. The x-coordinate of the SW surface location, $x_S(r, t)$, changes with the velocity of the SW motion $U_S \cos\theta - u(r)$,

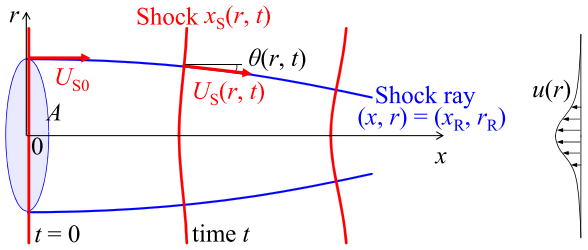

FIG. 5. SW deformation model by a local flow disturbance $u(r)$ with the SW surface location x_S (red) and SW ray trajectory (x_R, r_R) (blue).

where the propagation velocity of the deformed SW is $U_S(r, t) = M_S(r, t)a$. Note that $M_S(r, t)$ is the shock Mach number of the deformed SW and U_S is the velocity perpendicular to the deformed SW surface.

U_S can be represented by $U_S = U_{S0} + \delta U_S$ with the perturbation δU_S induced by the SW deformation. δU_S is related to the modulated overpressure. When the change in the overpressure due to velocity disturbance is given by p_{rms} listed in Table I, δU_S estimated from the Rankine-Hugoniot relations is about $u_{rms}/10^1$ ($\approx U_{S0}/10^4$). Therefore, for simplicity, we assume that the SW movement velocity in the x direction is given by $U_S \cos\theta - u(r) \approx U_{S0} - u(r)$, where the weak deformation is considered ($\theta(r, t) \ll 1$). We can derive the SW surface location $x_S(r, t) = (U_{S0} - u(r))t$, where the initial location of the SW is $x_S(r, 0) = 0$. Then, $\theta(r, t)$ is given by

$$\tan\theta(r, t) = \partial x_S/\partial r = -u'(r)t, \tag{1}$$

where $u'(r) = du/dr$. Now, we consider the trajectory of the shock ray $(x_R(t), r_R(t))$, which is orthogonal to the SW surface: $dr_R/dx_R = -\tan\theta(r_R, t)$. Since the SW surface satisfies Eq. (1), the trajectory is

$$\frac{dr_R}{dx_R} = u'(r_R)t = \frac{x_R u'(r_R)}{U_{S0} - u(r_R)}. \tag{2}$$

With the initial location $(x_R, r_R) = (0, r_0)$, $U_{S0} \gg u_{rms}$, and $u(r) = u_{rms}f(\tilde{r})$, Eq. (2) yields

$$\frac{x_R}{L} \approx \sqrt{2\frac{U_{S0}}{u_{rms}}\int_{\tilde{r}_0}^{\tilde{r}_R}\frac{d\tilde{r}^*}{f'(\tilde{r}^*)}}, \tag{3}$$

where $\tilde{r}_0 = r_0/L$ and $\tilde{r}_R = r_R/L$.

Since $dM_S/dA < 0$ ($dM_S/dr_R < 0$)[10] and Δp across the SW increases with M_S, we have $d(\Delta p)/dr_R < 0$, which is consistent with previous studies of the relation between the SW overpressure modulation and its deformation (e.g., the work of Kim *et al.*[7]). When $U_{S0} \gg |u|$ as in our experiments, the sign of dr_R/dx_R, Eq. (2), is determined by u'. When $u > 0$, $u' < 0$ as in the case of Fig. 5, resulting in $dr_R/dx_R < 0$. Thus, as the SW propagates (x_R increases) in the turbulence with $u > 0$, r_R decreases, resulting in the increase in the overpressure and shock Mach number because of $dM_S/dr_R < 0$. In a similar way, $u < 0$ results in the decrease in M_S and Δp. Thus, the present model of the SW modulation also predicts the positive correlation observed in Fig. 2.

Since $|dr_R/dt|$ monotonically increases from $|dr_R/dt| = 0$ at $t = 0$, the change in r_R and Δp at the earlier time is much slower than the later time. The change in Δp in the model becomes large after a certain period of time, which is called the response time in this letter. During this time period, the SW propagates over a certain distance called the response distance. Thus, the model is also consistent with our experimental finding of the finite response time, which is confirmed with the high correlation away from the wall in our experiments.

We denote the response time and distance by t_p and x_p, respectively. Because x_p is given by $x_p = x_R(t_p)$, where x_R follows Eq. (3) with $r_R(t_p)$, we can easily derive the following scaling law for the response distance x_p:

$$x_p/L \propto (u_{rms}/U_{S0})^{-0.5} = (M_T/M_{S0})^{-0.5}, \tag{4}$$

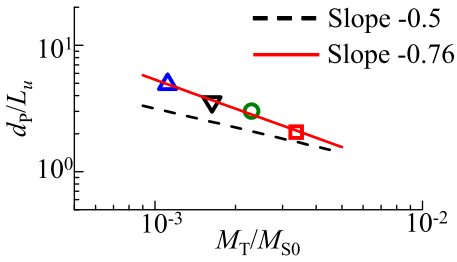

FIG. 6. Relation between d_P/L_u and M_T/M_{S0}. Broken line shows Eq. (4). See Table I for symbols.

where $M_T = u_{rms}/a$ is the turbulent Mach number. It should be noticed that the SW deformation in the model is caused by the fluid deformation by the shear $du(r)/dr$. The shear time scale for $u(r)$ is given by $t_e = L/u_{rms}$, which is also known as the large-eddy turnover time. Then, we have a scaling for the response time t_p, which is equivalent to Eq. (4),

$$t_p/t_e \propto (M_T/M_{S0})^{0.5}. \quad (5)$$

In Fig. 6, the response distance estimated as d_P is compared with Eq. (4), where d_P/L_u is plotted against M_T/M_{S0} (L_u is used here since L is proportional to L_u in the grid turbulence[8]). d_P/L_u decreases with M_T/M_{S0} with the power law $d_P/L_u \propto (M_T/M_{S0})^{-0.76}$, which is fairly close to the prediction in Eq. (4) obtained by a very simple model of the shock deformation due to a local flow disturbance.

In summary, we have experimentally confirmed the finite response time of the post-SW overpressure modulation due to turbulence. The modulation is induced by the large-scale turbulent motions around the SW ray, while the turbulence influences become significant in the post-SW overpressure after it propagates over a certain distance (response distance). We have also proposed a simple model for the modulation based on the small deformation of the SW by a local flow disturbance, in which the response time is related to the small-deformation time scale of the SW. The model well explains the correlation between the turbulence velocity fluctuation and the peak-overpressure fluctuation behind the SW. This model predicts that the response time is proportional to the product of the large-eddy turnover time and $(M_T/M_{S0})^{0.5}$ while the response distance is given as the product of the SW propagation velocity and the response time. We have shown that the scaling for the response distance expected from the model is recovered fairly well in the experiments considering the simplicity of the model, providing a new framework to understand the shock/turbulence interaction based on the SW deformation.

This work was supported by JSPS KAKENHI, Grant Nos. 25289030 and 16K18013. The authors would like to thank Mr. S. Nishio, Drs. K. Mori, A. Iwakawa, Y. Ito, K. Iwano, and T. Kitamura for their help in the measurement system setup and their valuable comments.

[1]M.-M. Mac Low and R. S. Klessen, "Control of star formation by supersonic turbulence," Rev. Mod. Phys. **76**, 125 (2004).
[2]V. A. Thomas and R. J. Kares, "Drive asymmetry and the origin of turbulence in an ICF implosion," Phys. Rev. Lett. **109**, 075004 (2012).
[3]C. B. Pepper, M. A. Nascarella, and R. J. Kendall, "A review of the effects of aircraft noise on wildlife and humans, current control mechanisms, and the need for further study," Environ. Manage. **32**, 418–432 (2003).
[4]B. Lipkens and D. T. Blackstock, "Model experiment to study sonic boom propagation through turbulence. Part I. General results," J. Acoust. Soc. Am. **103**, 148–158 (1998).
[5]O. I. Dokukina, E. N. Terentiev, L. S. Shtemenko, and F. V. Shugaev, "Pressure fluctuations within a turbulent gas flow and their interaction with a shock wave," Moscow Univ. Phys. Bull. **68**, 118–122 (2013).
[6]A. Sasoh, T. Harasaki, T. Kitamura, D. Takagi, S. Ito, A. Matsuda, K. Nagata, and Y. Sakai, "Statistical behavior of post-shock overpressure past grid turbulence," Shock Waves **24**, 489–500 (2014).
[7]J. H. Kim, A. Sasoh, and A. Matsuda, "Modulations of a weak shock wave through a turbulent slit jet," Shock Waves **20**, 339–345 (2010).
[8]T. Kitamura, K. Nagata, Y. Sakai, A. Sasoh, O. Terashima, H. Saito, and T. Harasaki, "On invariants in grid turbulence at moderate Reynolds numbers," J. Fluid Mech. **738**, 378–406 (2014).
[9]F. Grasso and S. Pirozzoli, "Shock-wave–vortex interactions: Shock and vortex deformations, and sound production," Theory Comput. Fluid Dyn. **13**, 421–456 (2000).
[10]G. Whitham, "On the propagation of shock waves through regions of non-uniform area or flow," J. Fluid Mech. **4**, 337–360 (1958).